Geophys. J. Int. (2012) doi: 10.1111/j.1365-246X.2012.05394.x

Palaeomagnetism of the South Harghita volcanic rocks of the East Carpathians: implications for tectonic rotations and palaeosecular variation in the past 5 Ma

C.G. Panaiotu,[1] M. Vişan,[2] A. Ţugui,[3] I. Seghedi[2] and A. G. Panaiotu[1]

[1] *Paleomagnetic Laboratory, University of Bucharest, Bălcescu* 1, 010041 *Bucharest, Romania. E-mail: cristian.panaiotu@gmail.com*
[2] *Institute of Geodynamics, Romanian Academy, Jean-Luis Calderon* 19-21, 020032*, Bucharest, Romania*
[3] *National Institute for Earth Physics, Bucharest-Măgurele, Romania*

Accepted 2012 January 23. Received 2012 January 19; in original form 2011 August 4

SUMMARY

Lavas of Pliocene–Quaternary age were sampled in the South Harghita Mountains, which form the southern end of the Călimani–Gurghiu–Harghita volcanic chain of the East Carpathians. The analyses of 68 volcanic sites in the South Harghita Mountains provided 62 sites with well-constrained directional data ($n > 5$ and $k > 50$) in an age interval ranging from 0.5 to 4.3 Ma. The age and polarity for the 62 sites (38 normal and 24 reversed) are consistent with the Geomagnetic Reversal Time Scale and support the model of the southward migration of the volcanism. The distribution of the VGPs is Fisherian and the mean pole position, both from all contributing sites and from the 53 sites older than 2 Ma, includes the spin axis. This result is consistent with the absence of important vertical axis rotations after the emplacement of the volcanic rocks in agreement with tectonic models for the Pliocene–Quaternary evolution of the bending area of the East Carpathians. Virtual geomagnetic pole dispersions are consistently high compared with global values obtained between 40 and 55°N, but closer to the values obtained only from the Time Averaged geomagnetic Field Initiative studies for the same latitudinal band. Our data are compatible with the prediction of the statistical palaeosecular variation model TK03. The inclination anomaly is less than 1° in accord with the Total Average Field global data. These palaeomagnetic data from the South Harghita volcanic rocks are the first data from the southeastern Europe which can be considered in the databases for time averaged field and palaeosecular variation from lavas analyses in the last 5 Ma.

Key words: Palaeomagnetic secular variation; Palaeomagnetism applied to tectonics; Rock and mineral magnetism; Europe.

INTRODUCTION

In the eastern Carpathian–Pannonian region in the last 15 Ma, westward-dipping subduction in a land-locked basin caused collision of a lithospheric blocks coming from the west with the southeastern border of the European Plate (e.g. Seghedi *et al.* 2004; Schmid *et al.* 2008; van Hinsbergen *et al.* 2008; Ustaszewski *et al.* 2008). An important calc-alkaline and alkaline magmatism was closely related to subduction, rollback, collision and extension (Seghedi *et al.* 2004). In the East Carpathians this volcanic activity formed the Călimani–Gurghiu–Harghita (CGH) volcanic chain (Fig. 1). This volcanic chain is around 160 km long and the volcanic activity gradually migrated to the south between the Miocene (∼12 Ma) and the Quaternary (∼0.2 Ma; e.g. Pécskay *et al.* 1995). The last phase of volcanic eruptions (Pliocene–Quaternary, Pécskay *et al.* 2006) occurred in the South Harghita Mountains, which form the southern end of the CGH volcanic chain. This volcanism was coeval with the last peak of crustal deformation in the Carpathian bending zone (Merten *et al.* 2010). The deformation was characterized by coeval uplift in the orogen and subsidence in the foreland with similar amplitudes in the order of 2–4 km (Maţenco *et al.* 2010).

Palaeomagnetic studies performed in the 1970s covered mainly the central part of the CGH volcanic chain and reports only a five sites from the South Harghita Mountains (Pătraşcu 1976; Michailova *et al.* 1983). Main goals of this study are to characterize and quantify the possible existence of tectonic crustal block rotations during the final stage of deformation and to contribute to palaeosecular variation (PSV) from lavas and palaeomagnetic time-averaged field (TAF) with data from Europe. The tectonic implications of the palaeomagnetic results and their validity for geomagnetic studies are discussed.

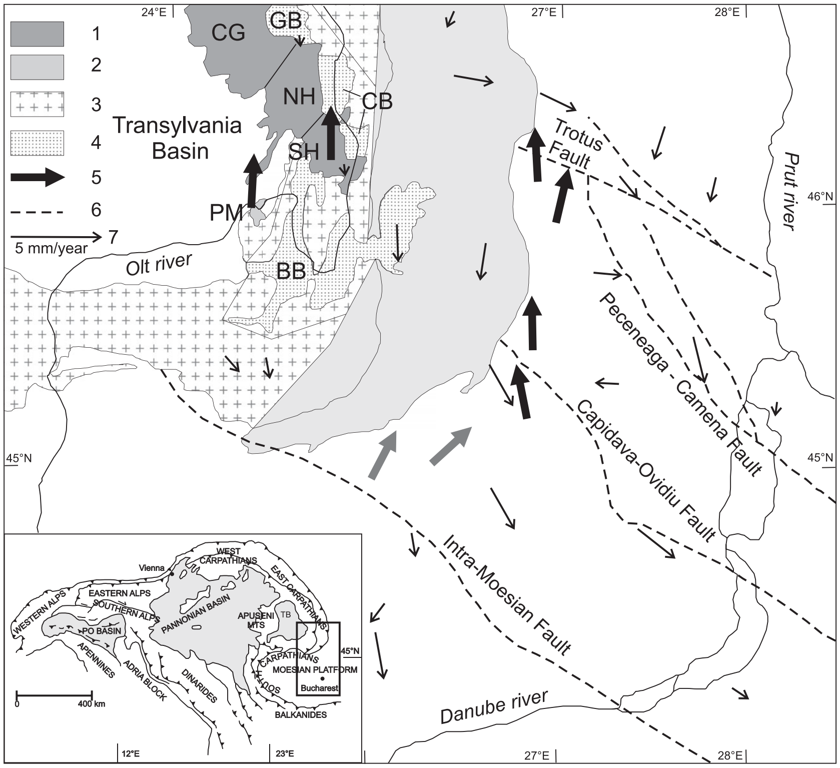

Figure 1. Geological sketch map of the bending area of the East Carpathians and surrounding areas (modified after Fielitz & Seghedi 2005). Symbols: 1, Miocene to Quaternary volcanic areas: Călimani-Gurghiu (CG), North Harghita (NT), South Harghita (SH) and Perşani Mountains (PM); 2, Moldavide nappes of the East Carpathians; 3, Dacides and other inner Carpathians nappes; 4, Miocene–Quaternary intramontane basins: Gheorgheni Basin (GB), Ciuc Basin (CB) and Braşov Basin (BB); 5, area mean palaeomagnetic declinations (this study and Dupont-Nivet *et al.* 2005): no rotation (black arrows), significant rotation (dark grey arrows); 6, present day seismic active faults in the Moesian Platform; and 7, measured GPS horizontal velocities with respect to Eurasian Plate (van der Hoeven *et al.* 2005).

GEOLOGICAL SETTING AND SAMPLING

The Alps, Carpathians and Dinarides (Fig. 1) form a topographically continuous, yet highly curved orogenic belt, which encircles the Pannonian Basin (Ustaszewski *et al.* 2008). They are part of the much larger system of Circum-Mediterranean orogens (e.g. Ustaszewski *et al.* 2008; van Hinsbergen *et al.* 2008; Seghedi & Downes 2011). The Pannonian Basin of Central and Eastern Europe was formed by rapid Miocene extension created by northeastward movement of the Adria block and collision with Europe (e.g. Lorinczi & Houseman 2010). The Miocene evolution of the Carpathians is mainly driven by the NE- and later E-ward retreat of a SW-, later W-dipping subduction zone (Sperner *et al.* 2001). During this tectonic episode the whole Intra-Carpathian area behaved as a uniform, but not rigid upper plate against the subducting European Plate (Panaiotu 1998; Csontos & Vörös 2004; Ustaszewski *et al.* 2008). The collision first took place in the northern part of the Carpathian arc, around 13 Ma, and later in the eastern part, around 11 Ma (e.g. Csontos & Vörös 2004). Post-11 Ma crustal deformation peaked near the limit between the Pliocene and Quaternary and was restricted to the area of the SE Carpathians (Maţenco *et al.* 2010). This complex tectonic history was accompanied by the generation of a wide variety of magmas that shows an age range from Miocene to Recent times (Pécskay *et al.* 2006). The main tectonic mechanisms during which magmas were generated imply both core-complex extension and transtensional faulting (Seghedi & Downes 2011). Blocks with weak lithosphere tended to break and disintegrate: magmas were formed above and at their boundaries (e.g. Pannonian basin, Seghedi & Downes 2011). Blocks with relatively strong lithosphere formed magmas at destructive boundaries along transtensional faults (e.g. the CGH volcanic chain at the eastern margin of the Transylvanian basin, Seghedi & Downes 2011).

South Harghita is the youngest portion of the CGH chain in the East Carpathians. Most of the CGH chain is situated between the Transylvanian Basin and East Carpathian Units, but South Harghita (Fig. 1) is different because volcanic edifices crosscut the easternmost tip of the Dacia flysch units (Szakács *et al.* 1993; Szakács & Seghedi 1995). A series of volcanic centres are concentrated along individual faults and/or at intersections of faults and the age of volcanism is gradually younger to the south, ranging from 5.1 to 0.02 Ma (Pécskay *et al.* 1995; Fielitz & Seghedi 2005). The geometry of the faults and alignment of volcanic centres indicate that both strike-slip and normal faulting permitted the ascent of magmas generated in the upper mantle and lower crust (Mason *et al.* 1996; Seghedi *et al.* 2004). The magmatism was coeval with development of the Ciuc Basin (Gîrbacea *et al.* 1998; Fielitz & Seghedi 2005) or post-dated the beginning of subsidence in the Braşov Basin (<5.8 Ma, Ciulavu *et al.* 2000). The main volcanic structures in the South Harghita Mountains are (Fig. 2): Luci-Lazu and Şumuleu-Ciuc volcanic structures [4.3 (5.1?)–3.6 Ma], Cucu volcanic structure (2.8–2.2 Ma), Pilişca volcanic structure (2.5–1.5 Ma), Malnaş and Bixad intrusive domes (2.2–1.4 Ma), Balvanyos extrusive domes (0.9–1.0 Ma) and Ciomadu volcanic structure (0.6–0.2 Ma).

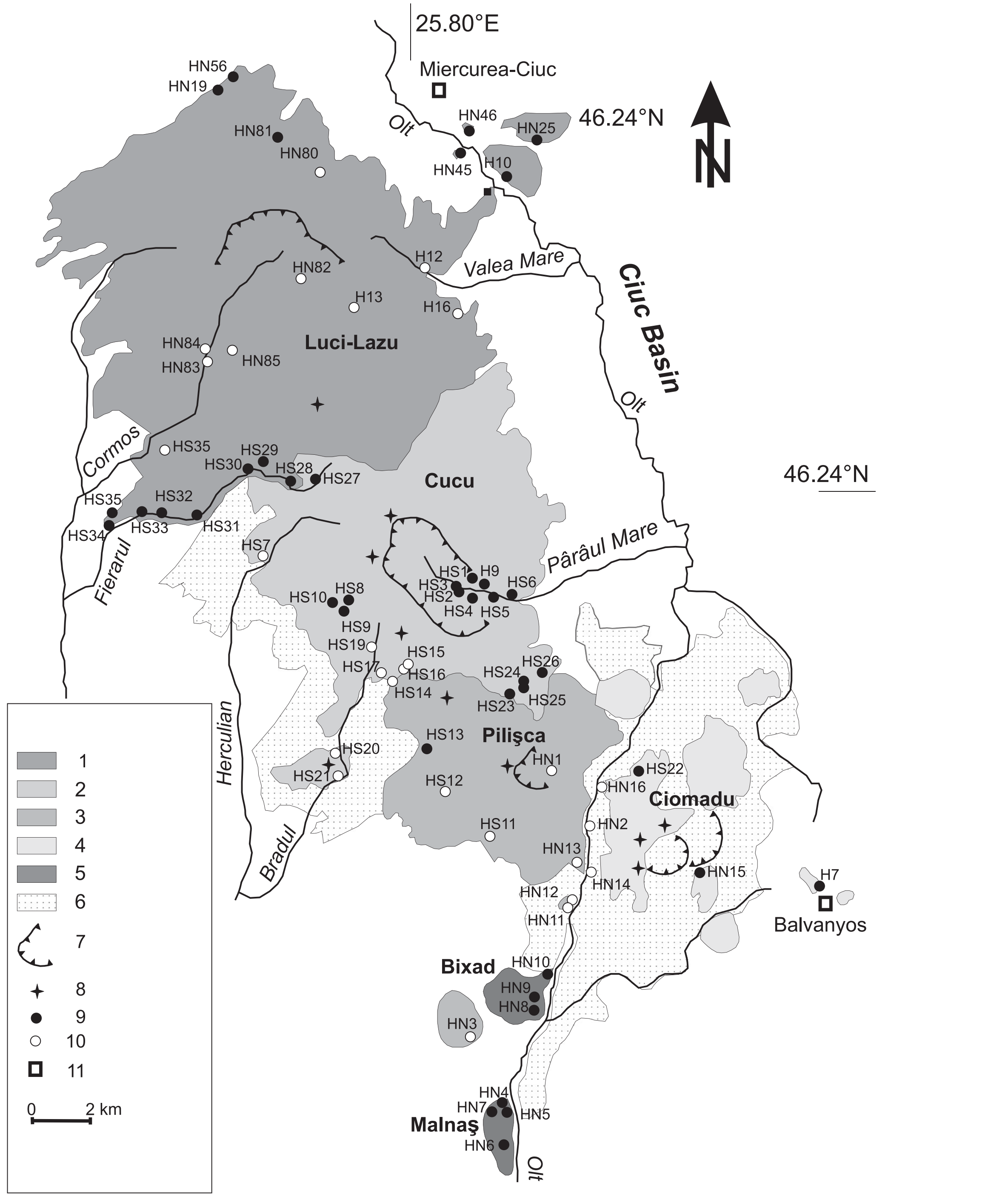

Figure 2. Location of sampling sites in the South Harghita volcanic area. Symbols: 1, Luci-Lazu volcanic and Şumuleu-Ciuc volcanic structure (4.3 (5.1?)–3.6 Ma); 2, Cucu volcanic structure (2.8–2.2 Ma); 3, Pilişca volcanic structure (2.5–1.5 Ma); 4, Ciomadu volcanic structure (0.6–0.2 Ma) and Balvanyos extrusive domes (0.9–1.0 Ma); 5, Malnaş and Bixad intrusive domes (2.2–1.4 Ma); 6, volcanoclastic rocks; 7, crater; 8, eruption centre; 9, palaeomagnetic site with positive inclination; 10, palaeomagnetic site with negative inclination; and 11, locality. Map is modified after Seghedi *et al.* (1987).

'Normal' calc-alkaline characterizes the volcanic activity of South Harghita up to 3.9 Ma (Luci-Lazu and Şumuleu-Ciuc volcanic structures), similar to the rest of the CGH chain. At *ca*. 3 Ma magma compositions changed to adakite-like calc-alkaline and continued until recent times (<0.03 Ma) interrupted at 1.6–1.2 Ma by generation of Na and K-alkalic magmas, signifying changes in the source and melting mechanism (Seghedi *et al.* 2011). K-alkalic volcanism (2.2–1.4 Ma) developed at Bixad/Malnaş close to the southward extension of the South Harghita chain. Na-alkalic volcanism (1.5–0.6 Ma) developed 40 km to the west in the Perşani Mountains (Downes *et al.* 1995; Panaiotu *et al.* 2004) as complex or individual volcanic centres arranged parallel to a ∼NNE–SSW normal fault system with the same orientation as the main normal faults of the Braşov Basin.

The gradual southward migration in time and emplacement of volcanic edifices along the CGH volcanic chain is explained by the slab break-off process (e.g. Mason *et al.* 1998; Seghedi *et al.* 1998). After this initial phase, the significant perturbations recorded in the magma composition are probably induced by changes in the source and melting mechanism (Seghedi *et al.* 2011). The contemporaneous generation of various melt compositions over a short time interval during Pliocene-Quaternary imply rapid changes in the post-collisional tectonic regime. The youngest Pliocene (2.8–1.6 Ma) and Quaternary (1–0.03 Ma) adakite-like volcanism is progressively concentrated to the southeastern edge of the CGH chain, where the final phases of the Carpathians collision process are now active (Popa *et al.* 2011).

We took samples from 68 sites (Fig. 2, Table 1). The sampling strategy was based on the regional geological map Odorhei, scale 1:200000, (Sǎndulescu *et al.* 1968) and the volcanological study of the CGH volcanic chain of Szakács & Seghedi (1995). The South Harghita Mountains are covered with forest so the number of outcrops suitable for a palaeomagnetic study is limited and lava flow successions are not available for sampling. The extensive forest road network allowed us to sample as uniformly and randomly as possible throughout the representative temporal windows and structural sectors. We sought outcrops that were as chemically unaltered as possible and *in situ* according to field observations. The sites were usually separated by hundreds of metres and at different elevations to try to avoid sampling the same lava multiple times. Sampling was carried out by drilling cores 2.5 cm in diameter using a handheld gasoline-powered engine with a water pump. The samples were oriented using a Brunton magnetic compass and a sun compass where possible. Each site consisted of 6–10 samples spaced over a significant area of outcrop. There was no visual indication of post-emplacement tilting of sampled sites.

PALAEOMAGNETIC METHODS

Laboratory analyses were carried out in the palaeomagnetic laboratory at the University of Bucharest. Standard palaeomagnetic specimens (11 cm^3) were cut from each core. Remanent magnetizations were measured using a JR6A spinner magnetometer (AGICO). Alternating-field (AF) demagnetization was done using a Magnon International static AF demagnetizer. AF demagnetization was performed in steps from 0 to 200 mT, with 10–15 steps per specimen. Thermal demagnetization was performed with a home build heater (triple mumetal shields, non-inductive processor control furnace, residual magnetic field less than 5 nT). The heater and the magnetometer are installed inside a set of three Helmholts coils used to reduce geomagnetic field in the working area to less than 300 nT. The susceptibility variation upon thermal treatment was measured on Bartigton MS2B system. Thermal demagnetization was performed in 50° steps starting at 150–450°C, followed by 25°C steps to the maximum unblocking temperature.

At least two pilot specimens from each site were subjected to detailed AF and thermal demagnetization. Due to the general agreement between the directions obtained from AF and thermal demagnetization, AF demagnetization was the preferred procedure for processing all the samples from each site. Demagnetization data were plotted on orthogonal demagnetization diagrams (Zijderveld 1967), and magnetization components were isolated by principal component analysis (Kirschvink 1980) using the Remasoft 3.0 software (Chadima & Hrouda 2006). The line fits were based on the following constrains: (1) minimum four demagnetization steps; (2) the line fit was anchored to the origin; and (3) the maximum angular deviation was less than 5°. Statistical analysis of directional data was done using Lisa Tauxe's PmagPy-2.51 software package (Tauxe 2011).

The hysteresis properties of at least one specimen per site were measured at room temperature using a VSM model 3900 (Princeton Measurements) with a maximum applied field of 1 T. The saturation magnetization (M_s), saturation remanent magnetization (M_{rs}) and coercive force (B_c) values were calculated after correction for the paramagnetic contribution. The coercivity of remanence (B_{cr}) and the ratio between isothermal remanent magnetization at 300 mT and M_{rs} (S ratio) were determined by applying a progressively increasing backfield after saturation. First-order reversal curve (FORC) diagrams were measured for selected specimens using the same instrument and processed with the FORCinel 1.18 software (Harrison & Feinberg 2008).

To further understand the magnetic properties the field dependence of the magnetic susceptibility between 2 and 700 A m^{-1} was determined for a specimen per site using the MFK1A kappabridge (AGICO). For representative specimens the temperature dependence of magnetic susceptibility was measured with a CS-L apparatus from liquid nitrogen temperature to room temperature and with CS4 apparatus from room temperature to 700°C. Both instruments were coupled with the MFK1A kappabridge. The heating–cooling cycle above room temperature was performed in argon atmosphere.

ROCK MAGNETIC RESULTS

Most sites (95 per cent) have a *S* ratio above 0.80, indicating a mineralogy dominated by low coercivity magnetic minerals. Field dependence of magnetic susceptibility shows no or a very small variation in all specimens (Fig. 3A). This behaviour is compatible with the presence of magnetite and/or titanium-poor titanomagnetite (Hrouda *et al.* 2006). The Curie temperature is a sensitive indicator of composition, which is useful in understanding the magnetic mineralogy. Low-field susceptibility versus temperature experiments were conducted to determine the Curie temperature on at least a sample from each site. All samples exhibit a T_c between 550 and 580°C, which indicates the presence of magnetite (Fig. 3B–D). In some samples (Fig. 3C) the drop in magnetic susceptibility is gradual starting at 500°C, which indicates the presence of titanium-poor titanomagnetite. In other samples we noted a decay of magnetic susceptibility between 350 and 450°C (Fig. 3D). We attributed this drop to the inversion of maghemite (e.g. Tauxe 2002). Verwey transition can be identified only in samples where magnetite is the only magnetic mineral (Fig. 3B).

The ratios of the hysteresis parameters plotted as a Day diagram (Day *et al.* 1977; Dunlop 2002) in Fig. 4(A) show that most grain sizes are scattered within the pseudosingle domain (PSD) range. The majority of FORC diagrams (Fig. 4B) are compatible with a mixture of single domain (SD) and multidomain (MD) grains (Roberts *et al.* 2000) in agreement with theoretical models which show that PSD behaviour is due to superimposed independent SD and MD moments (Dunlop 2002). The three sites with a *S*-ration below 0.6 have goose-necked hysteresis loops. This type of hysteresis loop is likely associated with mixtures of hematite and magnetite mineralogies (Tauxe *et al.* 1996).

DIRECTIONAL RESULTS

Natural remanent magnetization and demagnetization behaviour were measured on a total of 422 independent samples from 68 sites.

Table 1. Site locations and ages.

Site	Lat (°N)	Long (°E)	Alt (m)	Rock type	K–Ar Age (Ma)	Source for K–Ar age
Luci-Lazu and Şumuleu-Ciuc volcanic structures: 4.3 (5.1?)–3.6 Ma (Pécskay *et al.* 1995)						
HN46	46.34587	25.809	707	andesite		
HN45	46.33805	25.8026	659	andesite		
HN25	46.34067	25.84	762	andesite		
H10	46.32874	25.82281	685	andesite		
HN19	46.3604	25.6969	927	andesite		
HN56	46.3641	25.7005	900	andesite		
HN81	46.33493	25.7378	909	andesite		
HN80	46.33493	25.7378	909	andesite		
H12	46.3008	25.7901	771	dacite	4.14 ± 0.19	Peltz *et al.* 1987
H16	46.29243	25.80195	807	andesite	4.42 ± 0.26	Peltz *et al.* 1987
H13	46.2955	25.75445	996	andesite		
HN82	46.29468	25.7452	1091	andesite		
HN85	46.2785	25.6974	1019	andesite		
HN84	46.27655	25.6866	975	andesite		
HN83	46.27352	25.685	983	andesite		
HS35	46.245217	25.676017	887	andesite		
HS28	46.235917	25.724000	1119	andesite		
HS29	46.244583	25.712250	1088	andesite		
HS30	46.242467	25.705867	995	andesite		
HS31	46.232967	25.690150	903	andesite		
HS32	46.227767	25.671667	821	andesite		
HS33	46.230100	25.662700	748	andesite		
HS34	46.227250	25.653850	759	andesite	3.57 ± 0.61	Pécskay *et al.* 1995
HS36	46.230117	25.649183	773	andesite		
Cucu volcanic structure: 2.8–2.2 Ma (Pécskay *et al.* 1995)						
HS27	46.238233	25.744350	1233	andesite		
HS14	46.178017	25.769717	1007	andesite		
HS15	46.188550	25.781100	1122	andesite	2.51 ± 0.10	Szakács *et al.* 1993
HS16	46.187250	25.780817	1093	andesite		
HS17	46.178800	25.769483	981	andesite		
HS19	46.186717	25.762067	1032	andesite		
HS7	46.216267	25.714883	1078	andesite		
HS23	46.174567	25.821550	955	andesite		
HS24	46.176517	25.828050	892	andesite		
HS25	46.176783	25.829517	915	andesite		
HS26	46.179067	25.832400	885	andesite		
H9	46.206760	25.812720	949	andesite		
HS1	46.207633	25.810200	1007	andesite		
HS2	46.206383	25.807517	958	andesite		
HS3	46.206517	25.807450	973	andesite		
HS4	46.205600	25.808867	938	andesite		
HS5	46.204783	25.816417	895	andesite		
HS6	46.204600	25.820350	927	andesite	2.77 ± 0.13	Szakács *et al.* 1993
HS8	46.201850	25.748150	1139	andesite		
HS9	46.201700	25.746983	1093	andesite		
HS10	46.201067	25.742050	1082	andesite		
Pilişca volcanic structure: 2.5–1.5 Ma (Pécskay *et al.* 1995)						
HS13	46.155567	25.790283	955	andesite		
HN1	46.154310	25.846330	870	andesite		
HN2	46.137470	25.853790	622	andesite		
HN3	46.070050	25.804217	746	andesite		
HS20	46.216267	25.714883	743	andesite		
HS21	46.150000	25.749083	716	andesite		
HS12	46.142600	25.798450	927	andesite		
HS11	46.133800	25.818133	929	andesite		
HN11	46.107283	25.846283	604	andesite		
HN12	46.111383	25.846850	633	andesite		
HN13	46.126217	25.849683	646	andesite	2.42 ± 0.24	Peltz *et al.* 1987
HN16	46.149033	25.860733	691	andesite		
HN14	46.123200	25.854050	612	andesite		
Malnaş and Bixad intrusive domes: 2.2–1.4 Ma (Peltz *et al.* 1987)						
HN10	46.090933	25.837117	626	shoshonite		
HN4	46.052117	25.819400	632	shoshonite	2.22 ± 0.14	Peltz *et al.* 1987
HN5	46.051000	25.820317	612	shoshonite		
HN6	46.051000	25.820317	612	shoshonite		
HN7	46.048933	25.813267	643	shoshonite		
HN8	46.078133	25.833067	601	shoshonite		
HN9	46.082550	25.834183	584	shoshonite		
Balvanyos extrusive domes: 0.9–1.0 Ma (Pécskay *et al.* 1995)						
H7	46.115433	25.957328	877	dacite	1.02 ± 0.15	Pécskay *et al.* 1995
Ciomadu volcanic structure: 0.6–0.2 Ma (Pécskay *et al.* 1995)						
HS22	46.150033	25.879617	1058	dacite		
HN15	46.120767	25.903083	1105	dacite	0.56 ± 0.11	Szakács *et al.* 1993

Notes: Lat, Long: site coordinates. Alt; site altitude.

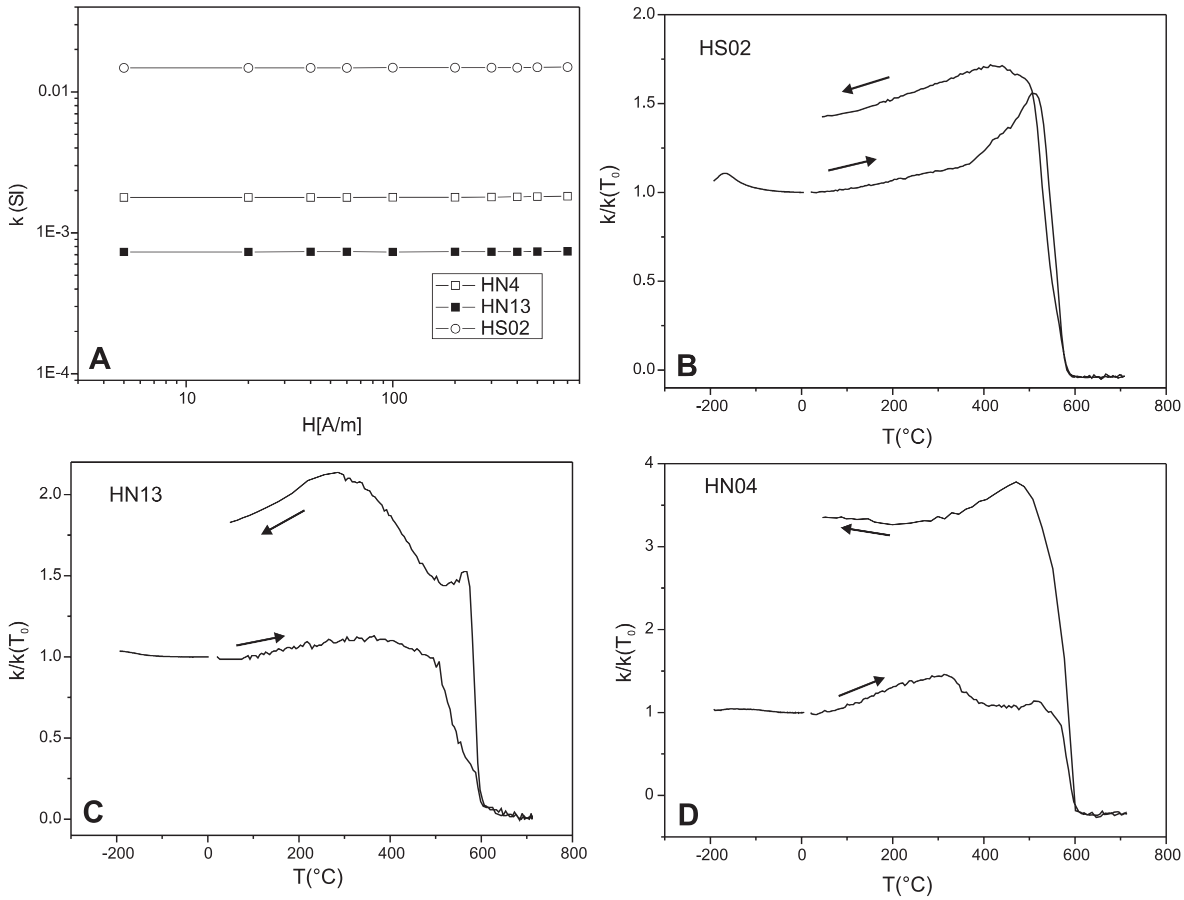

Figure 3. Typical examples of field (H) dependence and temperature (T) dependence of magnetic susceptibility (k).

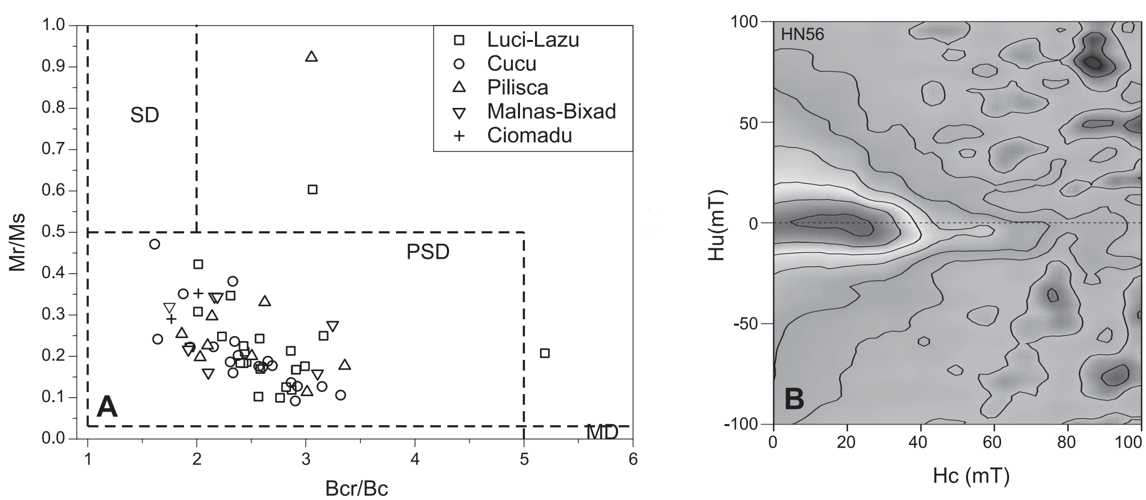

Figure 4. (A) Day plot of site-representative samples. The boundaries between SD, PSD and MD regions after Dunlop (2002); (B) Typical FORC diagram.

Typical step-wise demagnetization patterns from AF and thermal experiments (Fig. 5) show that for most samples fields of 10–20 mT were sufficient to remove a weak viscous component and successive higher fields produced linear principal component vectors that trend toward the origin. Thermal demagnetization has produced results that are indistinguishable from those obtained from other specimens at the same site using AF demagnetization. The distribution of blocking temperatures is in agreement with the magnetic mineralogy revealed by rock magnetic measurements. AF demagnetization was the preferred technique for magnetically cleaning the rest of the collection.

The mean site directions were obtained by averaging the AF and thermal results using Fisher statistics (Fisher 1953). A summary of site mean directions is presented in Table 2 and plotted in Fig. 6. According to the study of Johnson *et al.* (2008) we define site quality selection criteria for further analyses as n (number of samples) > 5 and k (precision parameter from Fisher statistics) > 50. Only one site (HN16) from 68 did not pass these criteria because it has only

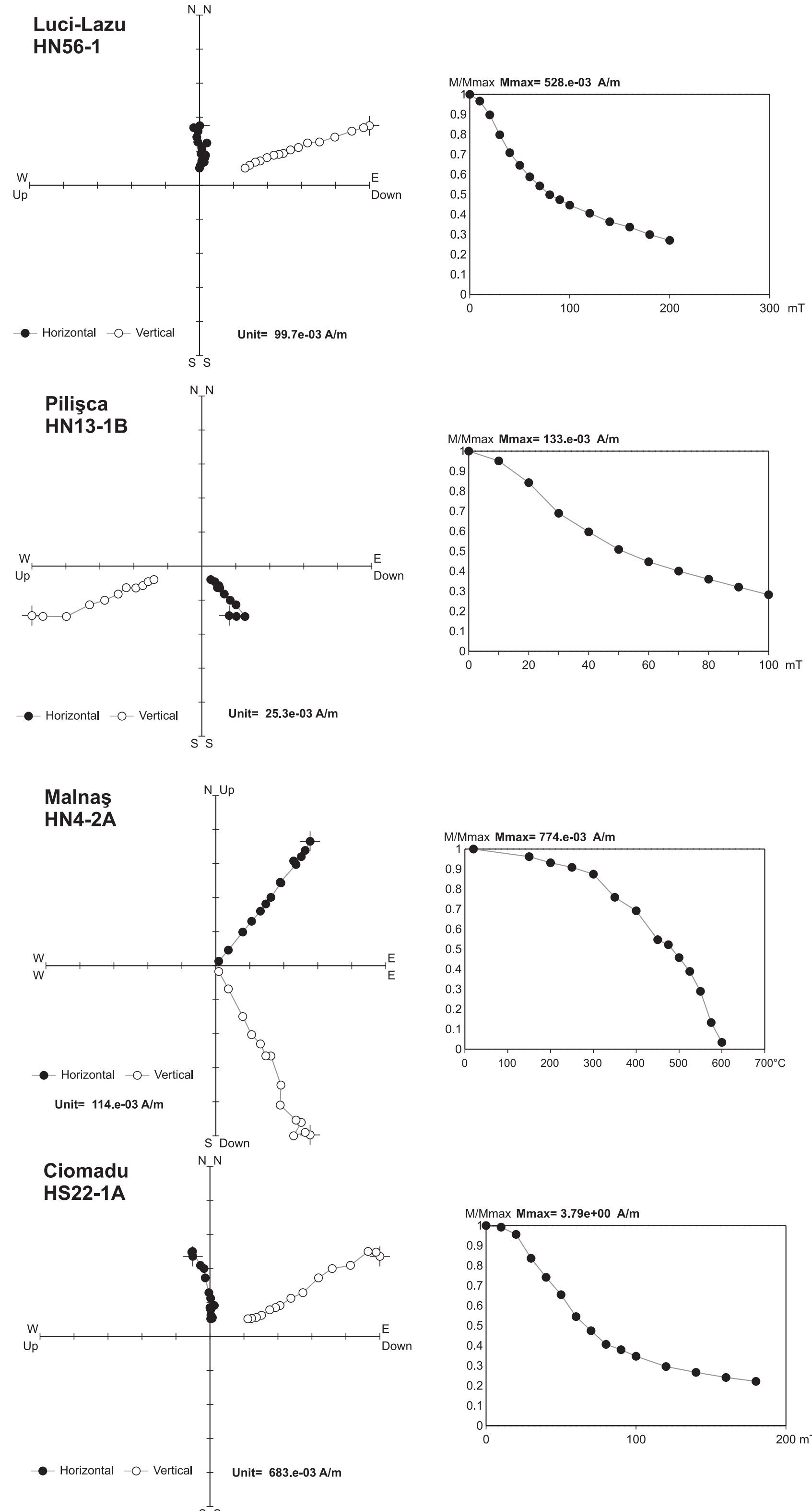

Figure 5. Orthogonal projections and decay curves showing typical demagnetization behaviour.

four samples. However the polarity and site mean direction of this site are in agreement with neighbouring sites with similar age. Most sites (65) also pass the more stringent criteria described by Tauxe *et al.* (2003), which demands $k > 100$. All selected sites with $k > 50$, have $\alpha_{95} < 10^{\circ}$, which is in agreement with cut-off values for PSV studies proposed by Opdyke *et al.* (2010).

Further statistical analysis of the directional data requires the removal of sites with transitional directions associated with low

Table 2. Palaeomagnetic results from the South Harghita volcanic area.

Site	*D* (°)	*I* (°)	*N*	*k*	α_{95} (°)	P	Plat (°)	PLon (°)
Luci-Lazu volcanic and Şumuleu-Ciuc volcanic structure: 4.3 (5.1?)–3.6 Ma								
HN46	307.0	38.0	7	195	4.3	T	40.6	284.1
HN45	337.0	60.5	7	666	2.3	N	72.8	322.5
HN25	287.4	30.0	7	83	6.6	T	23.5	294.8
H10	325.4	44.7	6	260	4.2	N	56.1	−88.3
HN19	345.6	67.7	6	227	4.5	N	79.6	−35.0
HN56	359.7	68.9	5	1031	2.4	N	84.0	24.1
HN81	335.0	61.9	5	616	3.1	N	72.0	−65.5
HN80	141.6	−15.1	5	101	7.7	T	−39.2	78.4
H12	194.4	−50.8	6	130	5.9	R	−71.5	−16.1
H16	185.0	−56.0	8	337	3	R	−79.6	3.0
H13	197.3	−54.5	5	368	4	R	−72.8	−29.7
HN82	203.6	−42.0	6	57	8.9	R	−60.9	337.0
HN85	173.3	−45.0	5	167	5.9	R	−69.6	43.1
HN84	167.9	−49.6	5	103	7.6	R	−71.6	60.5
HN83	186.5	−60.9	5	217	5.2	R	−83.6	−23.9
HS35	191.4	−53.7	6	369	3.5	R	−75.2	−14.0
HS28	35.4	51.9	7	889	2	N	59.7	130.0
HS29	41.0	58.1	8	315	3.1	N	59.2	114.8
HS30	24.8	62.7	7	123	5.5	N	72.4	113.9
HS31	343.2	63.2	7	335	3.3	N	78.2	−65.8
HS32	352.7	53.8	6	320	3.7	N	76.9	−126.8
HS33	340.8	56.9	7	620	2.4	N	73.3	−89.2
HS34	4.0	33.7	5	125	6.9	N	62.0	−162.5
HS36	343.3	43.6	7	332	3.3	N	65.3	−116.0
Cucu volcanic structure: 2.8–2.2 Ma								
HS27	341.6	53.0	7	137	5.2	N	71.1	−99.8
HS14	157.6	−71.9	5	284	4.5	R	−76.5	−169.9
HS15	115.2	−56.3	5	186	5.6	R	−47.7	130.1
HS16	108.9	−72.1	7	142	5.1	R	−46.7	157.3
HS17	149.0	−68.4	7	218	4.1	R	−69.1	142.3
HS19	139.2	−79.1	7	143	5.1	R	−59.5	178.3
HS7	124.6	−80.2	8	125	5.0	R	−54.2	178.3
HS23	18.1	83.6	6	116	6.2	N	58.0	33.2
HS24	297.2	76.2	5	271	4.6	N	51.9	−13.5
HS25	12.4	86.0	7	289	3.6	N	53.9	28.7
HS26	6.8	84.3	6	385	3.4	N	57.4	28.3
H9	16.7	46.6	6	123	6.0	N	67.4	164.4
HS1	9.1	44.0	8	183	4.1	N	68.4	−176.8
HS2	35.1	72.3	8	172	4.2	N	65.9	75.2
HS3	6.4	63.0	7	185	4.4	N	85.2	134.6
HS4	7.6	72.4	6	305	3.8	N	77.7	45.2
HS5	0.6	67.2	5	157	6.1	N	84.7	78.1
HS6	13.6	48.6	7	225	4.0	N	70.3	168.7
HS8	352.1	51.2	5	129	6.8	N	74.4	−128.4
HS9	358.9	60.4	6	150	5.5	N	85.1	−144.3
HS10	12.6	62.9	7	109	5.8	N	80.9	123.2
Pilişca volcanic structure: 2.5–1.5 Ma								
HS13	49.1	62.3	6	272	4.1	N	55.6	101.9
HN1	154.2	−41.7	5	202	5.4	R	−59.7	77.8
HN2	171.7	−60.4	6	217	4.6	R	−82.3	80.2
HN3	151.0	−11.1	7	163	4.7	T	−42.4	66.6
HS20	141.3	−64.5	7	249	3.8	R	−63.5	130.5
HS21	178.2	−59.2	7	168	4.7	R	−83.7	38.2
HS12	181.4	−62.8	7	126	5.4	R	−87.9	−1.7
HS11	164.6	−67.2	7	357	3.2	R	−79.0	141.8
HN11	167.9	−60.5	5	88	8.2	R	−77.2	88.4
HN12	130.8	−68.6	5	536	3.3	R	−57.8	144.4
HN13	136.9	−72.1	6	236	4.4	R	−61.6	154.3
HN16	157.8	−53.1	4	45	13.8	R	−69.1	87.3
HN14	156.1	−73.9	5	490	3.5	R	−70.2	169.3

Table 2. (*Continued*).

Site	D (°)	I (°)	N	k	α_{95} (°)	P	Plat (°)	PLon (°)
Malnaş and Bixad intrusive domes: 2.2–1.4 Ma								
HN10	114.3	81.5	5	136	6.6	T	37.5	45.0
HN4	38.9	52.2	8	594	2.3	N	57.6	126.0
HN5	36.0	48.2	5	112	7.2	N	57.3	134.1
HN6	47.0	44.1	5	405	3.8	N	47.7	127.7
HN7	30.5	48.3	6	430	3.2	N	60.9	140.3
HN8	35.5	47.6	5	283	4.6	N	57.3	135.4
HN9	32.6	50.9	6	151	5.5	N	61.1	134.3
Balvanyos extrusive domes: 0.9–1.0 Ma								
H7	18.4	73.5	9	804	1.5	N	72.8	58.9
Ciomadu volcanic structure: 0.6–0.2 Ma								
HS22	0.1	69.5	8	230	3.7	N	83.0	26.4
HN15	33.3	63.9	5	147	6.3	N	66.9	105.1

Notes: D, I, mean-site direction (declination, inclination); N, number of samples; k, α_{95}, Fisher's precision parameters and semi-angle of 95 per cent confidence; P, polarity (N = normal, R = reversed, T = transitional); Plat, Plon, corresponding VGP longitude and latitude.

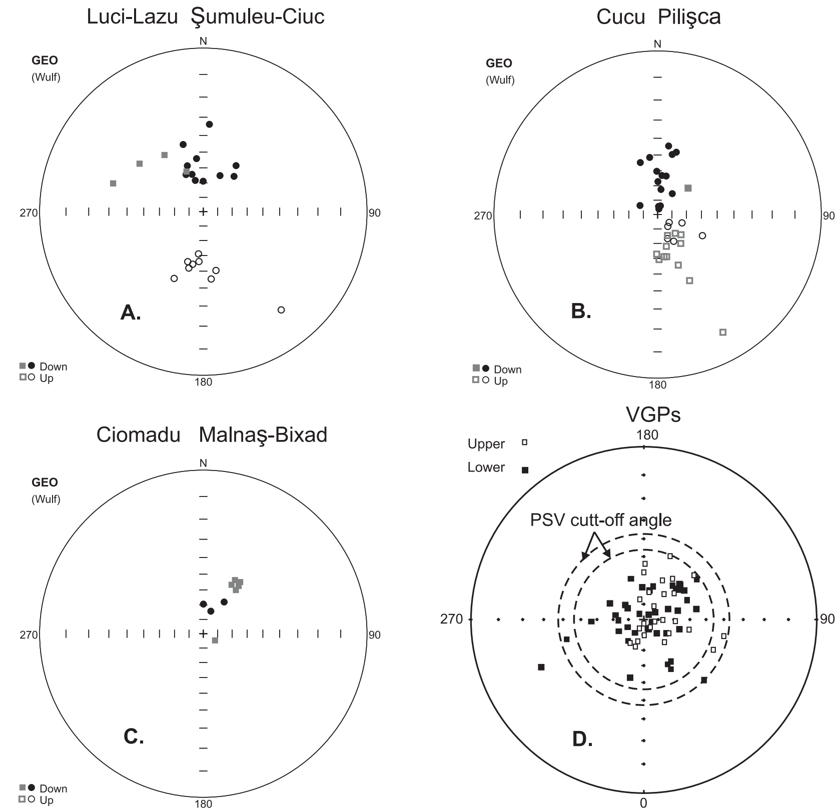

Figure 6. Site-mean directions and VGPs distribution: (A) Luci-Lazu (circles) and Şumuleu Ciuc (squares) volcanic structures; (B) Cucu (circles) and Pilişca (squares) volcanic structures; (C) Malnaş-Bixad intrusive domes (squares) and Ciomadu volcanic structure and Balvanyos dome (circles); and (D) VGPs distribution and PSV cut-off angles.

virtual geomagnetic pole (VGP) latitudes. We used two approaches to identify these sites: (1) a constant VGP latitude cut-off of 45° (e.g. Johnson *et al.* 2008); (2) the variable latitude cut-off based on the Vandamme (1994) criterion. A constant VGP latitude cut-off of 45° has removed five sites. Using the Vandamme criterion resulted in a cut-off value of 37.5, which removed one site. The two data sets have similar area mean VGP positions and statistics: (1) 45° cut-off latitude: latitude = 89.3°N, longitude = 87.7°, $k = 11.5$, $\alpha_{95} = 5.6°$; and (2) 37.5° cut-off latitude: latitude = 89.0°N, longitude = 288.7°, $k = 9.6$, $\alpha_{95} = 5.9°$. To facilitate the comparison with PSV data from Johnson *et al.* (2008) we decided to use their solution: constant cut-off latitude of 45°. This VGP data set has the longitudes uniformly distributed and the colatitudes exponentially distributed as required by the Fisher distribution (Tauxe 2002).

MAGNETIC POLARITY DATA

Geographic distribution of the magnetic polarities is presented in Fig. 2. In the Luci-Lazu volcanic structure we have identified 13 sites with normal polarity, 8 sites with reversed polarity and 3 sites with transitional directions. According to available K–Ar ages (Pécskay *et al.* 1995) the volcanism started in the northern part of the area and migrated gradually toward the south. The areal distribution of sites with normal and reversed polarities is in agreement with geographic and time distribution of these ages and polarity timescale (Fig. 7). The volcanism probably started during chron C3n and ended in subchron C2An3n.

In the Cucu volcanic structure 15 sites have normal polarity and 6 sites have reversed polarity. Taking into account the K–Ar ages the volcanic activity started during chron C2An1n and continued during chron C2r (Fig. 7). The Pilişca volcanic structure is dominated by reversed polarity sites (12 sites from 13). The dominance of reversed polarity is in agreement with K–Ar ages, which suggest eruptions during chrons C2r and C1r2r (Fig. 7). The reversed site mean directions from the Pilişca structure are relatively well-grouped even though they are geographically distributed within the structure. Because they plot in the same area as the reversed directions from the Cucu structure (Fig. 6B) it can be interpreted as an indication of dominant eruptions during chron C2r. Overall the distribution of magnetic polarities in the Cucu and Pilişca volcanic structures is compatible with southward migration of volcanism suggested by the distribution of K–Ar ages.

In the subvolcanic domes from Malnaş and Bixad we have identified only sites with normal polarity. Most of directions are well grouped (Fig. 6C), which suggests that both domes cooled during the same magnetic chron. Taking into account the confidence limits for the two K–Ar ages from the Malnaş dome (Fig. 7), the most probable time of emplacement, which fit the observed normal polarity, is during chron C2n (1.778–1.945 Ma, Lourens *et al.* 2004) . Seghedi *et al.* (2011) consider that the age of K-alkalic volcanism developed at Malnaş and Bixad is around 1.6–1 Ma. Our interpretation makes this K-alkalic volcanism slightly older: between 1.77 and 1.95 Ma. This minor age modification did not change the hypothesis of Seghedi *et al.* (2011) that the time of eruption of these K-alkalic magmas coincides with, or slightly post-dates, the onset of the latest Pliocene–Quaternary inversion in the bending area of the East Carpathians.

The normal polarity obtained from the Balvanyos extrusive dome is in agreement with the K–Ar age supporting emplacement during subchron C1r1n (Jaramillo). The three sites from the Ciomadu volcanic structure have normal polarity in agreement with the K–Ar ages inside chron C1n (Brunhes).

The reversal test of McFadden & McElhinny (1990) is positive with classification C ($\gamma_o = 10.2^\circ > \gamma_c = 11.3^\circ$) for VGPs older than 2 Ma (29 normal polarity sites, 24 reversed polarity sites). When applied to all VGPs (38 normal polarity sites, 24 reversed polarity sites) the reversal tests is negative (observed angle $\gamma_o = 16.0^\circ >$ critical angle $\gamma_c = 10.9^\circ$). The failure of the test is probably produced by the particular distribution of directions younger than 1.9 Ma from Ciomadu volcanic structure and Malnaş-Bixad domes (Fig. 6C): seven sites from nine have the declination around 35°.

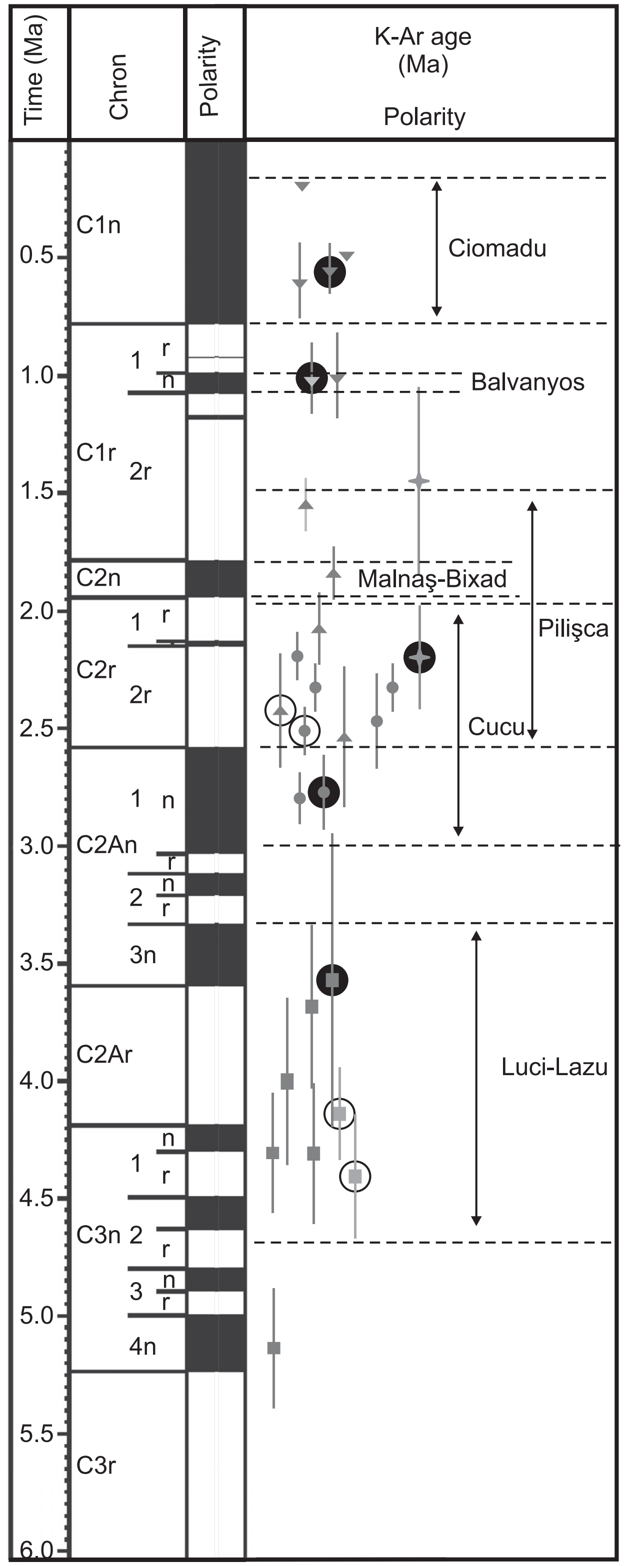

Figure 7. Correlation of main periods of volcanic activity with Geomagnetic Polarity Time Scale based on available K–Ar ages and geographic distribution of magnetic polarity. Large circles mark sites with both K–Ar age and magnetic polarity data (full circle, normal polarity; open circle, reversed polarity). Symbols for K–Ar ages: Luci-Lazu (squares), Cucu (circles), Pilişca (triangles), Malnaş and Bixad (stars), Ciomadu and Balvanyos (inverted triangles). Geomagnetic Polarity Time Scale is after Lourens *et al.* (2004).

TECTONIC IMPLICATION OF PALAEOMAGNETIC DATA

To detect effects of vertical-axis block rotations and tectonic deformation our palaeomagnetic results have to be compared with the palaeomagnetic data of similar age from stable Europe. Usually the reference palaeomagnetic poles are selected from Synthetic

Apparent Polar Wander Path (SAPWP) constructed for the major tectonic plates. In the last 10 yr three SAPWPs have been proposed for stable Europe: Besse & Courtillot (2002), Schettino & Scotese (2005) and Torsvik *et al.* (2008). All of these studies selected the palaeomagnetic poles to construct the SAPWPs mainly from different versions of the Global Palaeomagnetic Database (McElhinny & Lock 1990). They also used different kinematic rotation models for the last 5 Ma. Besse & Courtillot (2002) and Torsvik *et al.* (2008) used interpolated Euler rotation for ages younger than 5 Ma, but Schettino & Scotese (2005) used the model of current plate motions NUVEL-1A (DeMets *et al.* 1994). None of these studies have included the high quality palaeomagnetic data from the TAFI studies (Johnson *et al.* 2008). To detect small rotations we compute a palaeomagnetic reference pole for the last 5 Ma based on the area mean palaeomagnetic poles from the 17 TAFI studies (Johnson *et al.* 2008) and a recent palaeomagnetic pole from Mexico (Ruiz-Martínez *et al.* 2010). These palaeomagnetic poles were transferred to European coordinates using the kinematic model NUVEL-1A (DeMets *et al.* 1994) and their mean age. The new European reference pole for the last 5 Ma, based on 18 area-mean palaeomagnetic poles, has the following characteristics: latitude = 89.1°N, longitude = 185.1°, $k = 414$, $\alpha_{95} = 1.7$. This pole has better statistical parameters than those proposed by Besse & Courtillot (2002), Schettino & Scotese (2005) and Torsvik *et al.* (2008) for such young ages.

The amount of apparent rotation and poleward displacement have been evaluated using the method of Debiche and Watson (1995) and the software for palaeomagnetic analysis PMGSC4.2 (Enkin 2011). Results are listed in Table 3 both for the South Harghita volcanics and the Quaternary basalts from the Perşani Mountains. The mean VGP for the Perşani Mountains was computed after the exclusion of transitional data associated with the Cobb Mountain subchron and a later geomagnetic excursion (Panaiotu *et al.* 2004). The K–Ar age of these basalts is between 1.2 and 0.6 Ma (Panaiotu *et al.* 2004). Both the South Harghita Mountains and the Perşani Mountains apparent rotations and poleward displacement are small, lower or of the order of their uncertainties (Table 3). We can conclude that no significant vertical-axis rotations and tilting are detectable in these two areas from the Transylvanian basin after the emplacement of volcanic rocks.

Rotations younger than 5 Ma (Dupont-Nivet *et al.* 2005) are reported only in the external part of the bending area of the Carpathians (Fig. 1). The distribution of rotation presented in Fig. 1 is in agreement with geological model for the evolution of the bending area, which shows that post-11 Ma crustal deformation peaked near the limit between the Pliocene and Quaternary and was restricted to the area of the SE Carpathians (Cloetingh *et al.* 2004; Maţenco *et al.* 2010; Merten *et al.* 2010). In this context, it is interesting to note that these rotations are compatible with the present-day velocity field obtained from GPS, which is in good agreement with the Southeast Carpathians Pliocene–Quaternary geological evolution (van der Hoeven *et al.* 2005). Rotations in the last 5 Ma are observed only in the region southeast of the Carpathian bend zone (Fig. 1), between the Intra-Moesian Fault and the Capidava–Ovidiu Fault, which shows a present-day horizontal movement towards SSE of ~2.5 mm yr^{-1}. In the Transylvanian Basin, which shows very small motions with respect to Eurasia, the rotations are absent. Significant rotations are also absent in the external part of the bending area, between the Capidava–Ovidiu Fault and the Trotuş Fault where present-day GPS velocities are smaller and their directions are variable (Van der Hoeven *et al.* 2005).

PALAEOSECULAR VARIATION AND TIME-AVERAGE FIELD

We first examine the dispersion of VGPs recorded in the South Harghita Mountains with respect to regional compilations. The dispersion, S_B, was calculated using the equation from Johnson *et al.* (2008) and 95 per cent confidence limits estimated using a bootstrap resampling technique (Table 4). All computations were done using the PmagPy-2.73 software package (Tauxe 2011). The reverse polarity data has been flipped to its equivalent normal polarity. Since most of our data are older than 2 Ma we computed S_B both for all the sites and for sites older than 2 Ma. In the second case, we computed S_B both for normal and reversed polarities and the combined data set. Fig. 8(A) shows our results (Table 4) and regional compilations for the TAFI studies (Johnson *et al.* 2008, their Table 6) and global compilation (Johnson *et al.* 2008, their Table 8) in the latitudinal band 42–55°N. In this latitudinal band there are the nearest PSV data relevant for the sampling area latitude. For clarity in Fig. 8 we moved slightly the data with respect to their original latitude (around 0.1°). In the same figure we plotted the expected dispersion from PSV model G (McElhinny & McFadden 1997) and for the GAD version of the TK03 statistical model (Tauxe & Kent 2004). The VGP dispersions from our study are higher than the dispersion for the global compilation at 44.8°N latitude and the expected dispersion from model G. However, our results for rocks older than 2 Ma are in better agreement, at 95 per cent confidence level, with dispersions obtained from the TAFI studies at the latitude of 43°N and the TK03 model. It is interesting to note that the Matuyama data set presented by Johnson *et al.* (2008) shows several estimates of S_B around 53°N latitude that are higher than during the Brunhes, but similar to our results obtained at 46°N. Our results can be interpreted as an indication of a possible increase of VGP dispersion with time or alternatively regional differences in the PSV data sets at similar latitude (Johnson *et al.* 2008). However more data are needed at a global level to check if this is a real behaviour of the geomagnetic field or just reflect an incomplete database.

The second approach was to check if the distribution of directions from our study is compatible with the prediction from the statistical PSV model TK03. For this we used the ‘elongation/inclination’ or E/I method (Tauxe & Kent 2004). The result of this comparison is presented in Fig. 8(B). This figure was prepared using the PmagPy-2.73 software package (Tauxe 2011). The data from the Southern Harghita Mountains are consistent with the trend predicted by model TK03 in which all the non-axial dipole terms have zero mean. This agreement also shows that unrecognized tectonic tilting or other source of scatter besides the geomagnetic field did not play a role in our data (Tauxe *et al.* 2008), which support the use of data for detection of vertical axis rotations.

The TAF is examined using the inclination anomaly. Inclination anomaly is defined as the difference between the observed inclination and the expected inclination from a GAD at the same latitude (e.g. Johnson *et al.* 2008). The inclination anomaly (ΔI) is $0.2^\circ \pm 4.3^\circ$ for the whole data set and for the data set with ages between 2 and 4.5 Ma is $0.7^\circ \pm 4.3^\circ$. Taking into account the 95 per cent confidence limits these values are compatible with data for 0–5 Ma data set (Johnson *et al.* 2008) both for the latitude of 44.8°N ($\Delta I = -1.8^{\circ -0.1}_{-3.5}$) and 52.8°N ($\Delta I = 2.0^{\circ 3.3}_{0.7}$). Our data with almost no inclination anomaly can also be interpreted as a support for the trend observed in the global data by Johnson *et al.* (2008) which suggest a change from a negative inclination anomaly to a small positive inclination anomaly around 50°N. Both this very small

Table 3. Area means and tectonic motion.

Area	N	PLat (°)	PLon (°)	A_{95} (°)	R (°)	PD (°)
South Harghita (0.5–4.3 Ma)	62	89.6	58.5	5.6	0.1 ± 6.2	-1.2 ± 4.3
South Harghita (2–4.3 Ma)	53	85.5	310.1	5.6	6.9 ± 6.3	-1.8 ± 4.3
Perşani (0.6–1.2 Ma)	23	84.6	57.5	7.5	4.1 ± 8.8	-5.4 ± 5.7

Notes: N, number of VGPs; PLon, Plat, corresponding mean VGP longitude and latitude; A_{95}, semi-angle of 95 per cent confidence; R, apparent rotation; PD, poleward displacement.

Table 4. VGP dispersion and inclination anomaly for the South Harghita.

Latitude (°N)	Age (Ma)	Polarity	N	S_B (°)	S_B^{lo} (°)	S_B^{hi} (°)	ΔI (°)
46.02–46.36	0.5–4.3	All combined	62	24.1	21.3	26.5	0.2 ± 4.3
	2–4.3	All combined	53	23.1	20.4	25.9	0.7 ± 4.3
	2–4.3	Normal	29	22.9	18.8	26.5	0.3 ± 6.2
	2–4.3	Reversed	24	24.3	19.6	29.0	0.7 ± 6.3

Notes: N, number of sites; S_B, the between-site VGP dispersion, along with 95 per cent confidence limits (S_B^{lo}, S_B^{hi}); ΔI, inclination anomaly.

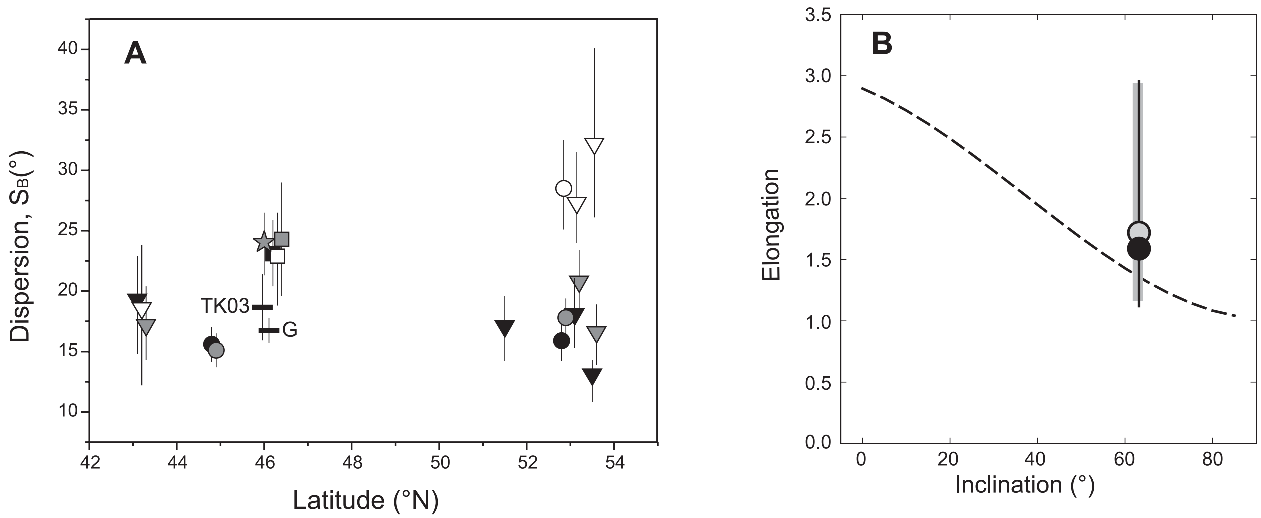

Figure 8. (A) VGP dispersion (S_B) and its 95 per cent confidence interval determined in the latitudinal band 42–55°N and predicted dispersions for Model G and TK03 (horizontal bars). Data from South Harghita (SH) are represented with: star, all data set, normal and reversed data combined; squares, data older than 2 Ma: normal polarity data (black), reversed polarity data (white), normal and reversed data combined (grey); Data from Johnson *et al.* (2008) are represented with full symbols for Brunhes-age normal polarity, open symbols for Matuyama-age reversed polarity data and grey symbols for combined normal and reversed polarity: inverted triangles represent data only from TAFI studies, circles are latitudinally binned global data. (B) Elongation–inclination plot of the South Harghita data (grey circle, all data; black circle, data older than 2 Ma) and their 95 per cent bootstrapped confidence boundary against prediction from model TK03 (dashed line).

inclination anomaly and the mean pole position, which is indistinguishable from the spin axis are consistent with field geometry with insignificant nonzero nonaxial dipole contributions (Tauxe *et al.* 2004).

CONCLUSIONS

The analyses of 68 volcanic sites in the South Harghita Mountains provided 62 high-quality new sites having well-constrained directional data ($n > 5$ and $k > 50$) and ages ranging from 0.5 to 4. 3 Ma. The distribution of the VGPs is Fisherian and the mean pole position, both from all contributing sites and from the 53 sites older than 2 Ma, includes the spin axis. This result is consistent with the absence of important vertical axis rotations after the emplacement of the volcanic rocks, which is in agreement with the tectonic models for the Pliocene–Quaternary evolution of the bending area of the Eastern Carpathians.

PSV is larger than the expected value for 45°N from the global compilation of Johnson *et al.* (2008), but closer to the value obtained only from the TAFI studies. Our data are compatible with the prediction of the statistical PSV model TK03 (Tauxe & Kent 2004). The inclination anomaly is less than 1° in accord with the global compilation of Johnson *et al.* (2008) and support an axial dipole only TAF.

ACKNOWLEDGMENTS

CGP and AT were supported by grant PNII-IDEI 974/2007 and MV was supported by grant PNII-IDEI 151/2007. AGP was partially supported by University of Bucharest, grant 19601.20/2011. We thank Kristin Lawrence and an anonymous reviewer for their helpful comments.

REFERENCES

Besse, J. & Courtillot, V., 2002. Apparent and true polar wander and the geometry of the geomagnetic field over the last 200 Myr, *J. geophys. Res.*, **107**(B11), 2300, doi:10.1029/2000JB000050.

Chadima, M. & Hrouda, F., 2006. Remasoft 3.0— a user-friendly paleomagnetic data browser and analyzer, *Travaux Géophysiques,* **XXVII,** 20–21.

Ciulavu, D., Dinu, C., Szakács, A. & Dordea, D., 2000. Neogene kinematics of the Transylvanian Basin (Romania), *AAPG Bull.,* **84**(10), 1589–1615.

Cloetingh, S.A.P.L., Burov, E., Maţenco, L., Toussaint, G., Bertotti, G., Andriessen, P.A.M., Wortel, M.J.R. & Spakman, W., 2004. Thermo-mechanical controls on the mode of continental collision in the SE Carpathians (Romania), *Earth planet. Sci. Lett.,* **218,** 57–76.

Csontos, L. & Vörös, A., 2004. Mesozoic plate tectonic reconstruction of the Carpathian region, *Palaeogeog. Palaeoclimat. Palaeoecol.,* **210,** 1–56.

Day, R., Fuller, M.D. & Schmidt, V., 1977. Hysteresis properties of titanomagnetites: grain-size and compositional dependence, *Phys. Earth planet. Int.,* **13,** 260–267.

Debiche, M.G. & Watson, G.S., 1995. Confidence limits and bias correction for estimating angles between directions with applications to paleomagnetism, *J. geophys. Res.,* **100**(B12), 22405–24429.

DeMets, C., Gordon, R.G., Argus, D.F. & Stein, S., 1994. Effect of recent revisions to the geomagnetic reversal time scale on estimate of current plate motions, *Geophys. Res. Lett.,* **21**(20), 2191–2194.

Downes, H. *et al*., 1995. Petrology and geochemistry of the late Tertiary/Quaternary mafic alkaline volcanism in Romania, *Lithos,* **35,** 65–81.

Dunlop, D.J., 2002. Theory and application of the Day plot (Mrs/Ms versus Hcr/Hc): 1. Theoretical curves and tests using titanomagnetite data, *J. geophys. Res.,* **107**(B3), 2056, doi:10.1029/2001JB000486.

Dupont-Nivet, G., Vasiliev, I, Langereis, C., Krijgsman, W. & Panaiotu, C., 2005. Neogene tectonic evolution of the South and East Carpathians constrained by paleomagnetism, *Earth planet. Sci. Lett.,* **236,** 374–386.

Enkin, R.J., 2011. Paleomagnetism data analysis version 4.2 (PMGSC4.2),: http://gsc.nrcan.gc.ca/sw/paleo_e.php (last accessed 2011 August 1).

Fielitz, W. & Seghedi, I., 2005. Late Miocene–Quaternary volcanism, tectonics and drainage system evolution in the East Carpathians, Romania, *Tectonophysics,* **410,** 111–136.

Fisher, R.A., 1953. Dispersion on a sphere, *Proc. R. Soc. Lond. Ser. A,* **217,** 295–305, doi:10.1098/rspa.1953.0064.

Gîrbacea, R., Frisch, W. & Linzer, H.-G., 1998. Post-orogenic uplift induced extension: a kinematic model for the Pliocene to recent tectonic evolution of the Eastern Carpathians (Romania), *Geol. Carpathica,* **49,** 315–327.

Harrison, R.J. & Feinberg, J.M., 2008. FORCinel: an improved algorithm for calculating first-order reversal curve distributions using locally weighted regression smoothing, *Geochem. Geophys. Geosyst.,* **9**(5), Q05016, doi:10.1029/2008GC001987.

van Hinsbergen, D.J.J., Dupont-Nivet, D., Nakov, R., Oud, K. & Panaiotu, C., 2008. No significant post-Eocene rotation of the Moesian Platform and Rhodope (Bulgaria): Implications for the kinematic evolution of the Carpathian and Aegean arcs, *Earth planet. Sci. Lett.,* **273,** 345–358.

van der Hoeven, A.G.A. *et al*., 2005. Observation of present-day tectonic motions in the Southeastern Carpathians: results of the ISES/CRC-461 GPS measurements, *Earth planet. Sci. Lett.,* **239,** 177– 184.

Hrouda, F., Chlupáčová, M. & Mrázová, S., 2006. Low-field variation of magnetic susceptibility as a tool for magnetic mineralogy of rocks, *Phys. Earth planet. Inter.,* **154,** 323–336.

Johnson, C.L. *et al*., 2008. Recent investigations of the 0–5 Ma geomagnetic field recorded by lava flows, *Geochem. Geophys. Geosyst.,* **9,** Q04032, doi:10.1029/2007GC001696.

Kirschvink, J.L., 1980. The least-squares line and plane and the analysis of palaeomagnetic Data, *Geophys. J. R. astr. Soc.,* **62,** 699–718.

Lorinczi, P. & Houseman, G., 2010. Geodynamical models of lithospheric deformation, rotation and extension of the Pannonian Basin of Central Europe, *Tectonophysics,* **492,** 73–87

Lourens, L., Hilgen, F., Shackleton, N.J., Laskar, J. & Wilson, D., 2004. The Neogene Period, in *A Geological Time Scale,* pp. 409–440, eds Gradstein, F.M., Ogg, J.G. & Smith, A.G., Cambridge University Press, Cambridge.

Mason, P., Downes, H., Thirlwall, M.F., Seghedi, I., Szakács, A., Lowry, D. & Mattey, D., 1996. Crustal assimilation as a major petrogenetic process in the East Carpathian Neogene and Quaternary continental margin arc, Romania, *J. Petrol.,* **37,** 927–959.

Mason, P.R.D., Seghedi, I., Szakács, A. & Downes, H., 1998. Magmatic constraints on geodynamic models of subduction in the Eastern Carpathians, Romania, *Tectonophysics,* **297,** 157–176.

Maţenco, L., Krezsek, C., Merten, S., Schmid, S., Cloetingh, S. & Andriessen, P.A.M., 2010. Characteristics of collisional orogens with low topographic build-up: an example from the Carpathians, *Terra Nova,* **22**(3), 155–165.

McElhinny, M.W. & Lock, J., 1990. Global palaeomagnetic data base project, *Phys. Earth planet. Inter.,* **63,** 1–6.

McElhinny, M.W. & McFadden, P.L., 1997. Palaeosecular variation over the past 5 Myr based on a new generalized database, *Geophys. J. Int.,* **131,** 240–252.

McFadden, P.L., & McElhinny, M.W., 1990. Classification of the reversal test in paleomagnetism, *Geophys. J. Int.,* **103,** 725–729.

Merten, S., Maţenco, L., Foeken, J.P.T., Stuart, F.M. & Andriessen, P.A.M., 2010. From nappe-stacking to out-of-sequence post-collisional deformations: cretaceous to Quaternary exhumation history of the SE Carpathians assessed by low-temperature thermochronology, *Tectonics,* **29**(3), TC3013, doi:10.1029/2009tc002550.

Michailova, N., Glevasskaia, A., Tsykora, V., Neştianu, T. & Romanescu, D., 1983. New paleomagnetic data for the Călimani, Gurghiu and Harghita volcanic Mountains in the Romanian Carpathians, *Ann. Inst. Geol. Geofiz.,* **63,** 112–124.

Opdyke, N.D., Kent, D.V., Huang, K., Foster, D.A. & Patel, J.P., 2010. Equatorial paleomagnetic time-averaged field results from 0–5 Ma lavas from Kenya and the latitudinal variation of angular dispersion, *Geochem. Geophys. Geosyst.,* **11,** Q05005, doi:10.1029/2009GC002863.

Panaiotu, C., 1998. Paleomagnetic constrains on the geodynamic history of Romania, *Rep. Geod.,* **7,** 205–216.

Panaiotu, C.G., Pécskay, Z., Hambach, U. Seghedi, I. Panaiotu, C.C., Itaya, C.E.T., Orleanu, M. & Szakács, A., 2004. Short-lived Quaternary volcanism in the Perşani Mountains (Romania) revealed by combined K-Ar and paleomagnetic data, *Geologica Carpathica,* **55,** 333–339.

Pătraşcu, S., 1976. Paleomagnetic study of some Neogene eruptive formations in the Calimani–Gurghiu–Harghita (Romania), *Rév. Roum. Géol. Géophys. Géogr. Ser. Géophys.,* **20,** 51– 63.

Pécskay, Z., Edelstein, O., Seghedi, I., Szakács, A., Kovacs, M., Crihan, M. & Bernad, A., 1995. K-Ar datings of the Neogene-Quaternary calc-alkaline volcanic rocks in Romania, *Acta Vulcanologica,* **7,** 53-63.

Pécskay, Z. *et al*., 2006. Geochronology of Neogene magmatism in the Carpathian arc and intra-Carpathian area, *Geologica Carpathica,* **57,** 511–530.

Peltz, S., Vâjdea, E., Balogh, K. & Pécskay, Z., 1987. Contributions to the chronological study of the volcanic processes in the Călimani and Harghita Mountains (East Carpathians, Romania), *D.S. Inst. Geol. Geofiz,* **72–73/1,** 323–338.

Popa, M., Radulian, M., Szakács, A., Seghedi, I. & Zaharia, B., 2011. New Seismic and Tomography Data in the Southern Part of the Harghita Mountains (Romania, Southeastern Carpathians): connection with Recent Volcanic Activity, *Pure appl. Geophys.,* in press, doi:10.1007/s00024-011-0428-6.

Roberts, A.P., Pike, C.R. & Verosub, K.L., 2000. FORC diagrams: A new tool for characterizing the magnetic properties of natural samples, *J. geophys. Res.,* **105,** 28461–28475.

Ruiz-Martínez, V.C., Urrutia-Fucugauchi, J. & Osete, M.L., 2010. Palaeomagnetism of the Western and Central sectors of the Trans-Mexican volcanic belt–implications for tectonic rotations and palaeosecular variation in the past 11 Ma, *Geophys. J. Int.,* **180,** s577–s595.

Săndulescu, M., Vasilescu, A., Popescu, A., Mureşan, M., Arghir-Drăgulescu, A. & Bandrabur, T., 1968. Geological map of Romania, sheet Odorhei (scale 1:200000), Geological Institute of Romania, Bucharest.

Schettino, A. & Scotese, C.R., 2005. Apparent polar wander paths for the major continents (200 Ma to the present day): a palaeomagnetic reference frame for global plate tectonic reconstructions, *Geophys. J. Int.,* **163,** 727–759.

Schmid, S., Bernoulli, D., Fügenschuh, B., Maţenco, L., Schefer, S., Schuster, R., Tischler, M. & Ustaszewski, K., 2008. The Alpine–Carpathian–Dinaridic orogenic system: correlation and evolution of tectonic units, *Swiss J. Geosci,* **101,** 139–183.

Seghedi, I., Szakács, U., Stoian, A.C. & Grabari, M.G., 1987. Trace elements geochemistry of the South Harghita volcanics (East Carpathians): calc-alkaline and shoshonitic associations, *D.S. Inst. Geol. Geofiz.,* **72-73/1,** 381–397.

Seghedi, I., Balintoni, I. & Szakács, A., 1998. Interplay of tectonics and Neogene post-collisional magmatism in the Intracarpathian area, *Lithos,* **45,** 483–499.

Seghedi, I. *et al*., 2004. Neogene-Quaternary magmatism and geodynamics in the Carpathian-Pannonian region: a synthesis, *Lithos,* **72,** 117–146.

Seghedi, I. & Downes, H., 2011. Geochemistry and tectonic development of Cenozoic magmatism in the Carpathian–Pannonian region, *Gondwana Res.,* **20**(4), 655–672.

Seghedi, I., Maţenco, L., Downes, H., Mason, P.R.D., Szakács, A. & Pécskay, Z., 2011. Tectonic significance of changes in post-subduction Pliocene–Quaternary magmatism in the south east part of the Carpathian–Pannonian Region, *Tectonophysics,* **502**(1–2), 146–157.

Sperner, B., Lorenz, F.P., Bonjer, K.-P., Hettel, S., Müller, B. & Wenzel, F., 2001. Slab break-off–abrupt cut or gradual detachment? New insights from the Vrancea Region (SE Carpathians, Romania), *Terra Nova,* **13,** 172–179.

Szakács, A. & Seghedi, I., 1995. The Călimani–Gurghiu–Harghita volcanic chain, East Carpathians, Romania: volcanological features, *Acta Volcanologica,* **7,** 145–153.

Szakács, A., Seghedi, I. & Pécskay, Z., 1993. Pecularities of South Harghita Mts. as terminal segment of the Carpathian Neogene to Quaternary volcanic chain, *Rév. Roum. Géologie,* **37,** 21–36.

Tauxe, L., 2002. *Paleomagnetic Principles and Practice,* Kluwer Academic Publisher, Dordrecht.

Tauxe, L., 2011. PmagPy, software package,: http://magician.ucsd.edu/Software/PmagPy/index.html (last accessed 2011 August 1).

Tauxe, L. & Kent, D., 2004. A simplified statistical model for the geomagnetic field and the detection of shallow bias in paleomagnetic inclinations: was the ancient magnetic field dipolar? in *Timescales of the Internal Geomagnetic Field,* Geophys. Monogr. Ser. Vol. 145, pp. 101–115, eds Channell, J.E.T., Kent, D.V., Lowrie, W. & Meert, J.G., American Geophysical Union, Washington, DC.

Tauxe, L., Mullender, T.A.T. & Pick, T., 1996. Potbellies, wasp-waists and superparamagnetism in magnetic hysteresis, *J. geophys. Res.,* **101,** 571–583, doi:10.1029/95JB03041.

Tauxe, L., Constable, C., Johnson, C.L., Koppers, A.A.P., Miller, W.R. & Staudigel, H., 2003. Paleomagnetism of the southwestern U.S.A. recorded by 0–5 Ma igneous rocks, *Geochem. Geophys. Geosyst.,* **4**(4), 8802, doi:10.1029/2002GC000343.

Tauxe, L., Luskin, C., Selkin, P., Gans, P. & Calvert, A., 2004. Paleomagnetic results from the Snake River Plain: contribution to the time-averaged field global database, *Geochem. Geophys. Geosyst.,* **5,** Q08H13, doi:10.1029/2003GC000661.

Tauxe, L., Kodama, K.P. & Kent, D.V., 2008. Testing corrections for paleomagnetic inclination error in sedimentary rocks: A comparative approach, *Phys. Earth planet. Inter.,* **169,** 152–165.

Torsvik, T.H., Müller, R.D., Van der Voo, R., Steinberger, B. & Gaina, C., 2008. Global Plate Motion Frames: toward a unified model, *Rev. Geophys.,* **46,** RG3004, doi:10.1029/2007RG000227.

Ustaszewski, K., Schmid, S.M., Fügenschuh, B., Tischler, M., Kissling, E. & Spakman, W., 2008. A map-view restoration of the Alpine-Carpathian-Dinaridic system for the Early Miocene, *Swiss J. Geosci,* **101**(Supplement 1), S273–S294.

Vandamme, D., 1994. A new method to determine paleosecular variation, *Phys. Earth planet. Inter.,* **85,** 131–142.

Zijderveld, J.D.A., 1967. A.C. demagnetization of rocks: analysis of results, in *Methods of Palaeomagnetism,* pp. 254–286, eds Collinson, D.W., Creer, K.M. & Runcorn, S.K., Elsevier, Amsterdam.